Acta Oceanol. Sin., 2025, Vol. 44, No. 11, P. 127–140
https://doi.org/10.1007/s13131-025-2542-9

Ammonia and nitrite oxidation dynamics in the Changjiang (Yangtze) River Estuary: linking with productivity and oxygen consumption

Zhen-Zhen Zheng[1, 2*], Yutan Wang[1], Guiyi Ma[3], Qianhui Li[3], Jin-Yu Terence Yang[4], Anshuai Lu[3], Sijing Kang[4], Moyang Li[4], Xiuli Yan[5], Min Nina Xu[2], Li-Wei Zheng[2], Ehui Tan[2*], Shuh-Ji Kao[2]

[1] School of Ecology, Hainan University, Haikou 570228, China

[2] School of Marine Sciences, State Key Laboratory of Marine Resources Utilization in South China Sea, Hainan University, Haikou 570228, China

[3] School of Marine Biology and Fisheries, Hainan University, Haikou 570228, China

[4] State Key Laboratory of Marine Environmental Science, College of Ocean and Earth Sciences, Xiamen University, Xiamen 361102, China

[5] Guangdong Provincial Key Laboratory of Marine Disaster Prediction and Prevention, Institute of Marine Sciences, Shantou University, Shantou 515063, China

Received 26 May 2025; accepted 23 July 2025

Abstract

Nitrification, the process by which ammonia is oxidized to nitrite (ammonia oxidation, AO) and subsequently to nitrate (nitrite oxidation, NO), plays a critical role in the nitrogen cycle by linking the oxidized and reduced forms of nitrogen. This process consumes dissolved oxygen, releases protons, and produces the potent greenhouse gas nitrous oxide (N_2O), rendering it highly relevant to various environmental challenges, especially in coastal seas with high anthropogenic nitrogen input. Despite its importance, research has predominantly focused on AO, with fewer studies simultaneously investigating ammonia oxidation rates (AOR) and nitrite oxidation rates (NOR). This study measured AOR and NOR using the ^{15}N tracer technique in the Changjiang (Yangtze) River Estuary (CRE) during the summer of 2022, a season when bottom-water hypoxia occurred frequently. Overall, our findings showed that AOR exceeded NOR across different estuarine conditions. Specifically, higher ammonium and total suspended matter (TSM) concentrations significantly boosted AOR. Notably, despite lower TSM levels compared to previous studies, AOR remained high, suggesting that smaller particles may offer more surface area for ammonia-oxidizing microorganisms. In addition, surface productivity, indicated by the concentration of chlorophyll *a* (Chl *a*), was positively correlated with bottom-water nitrification and oxygen consumption. This suggested that increased surface productivity could enhance deep-water microbial nitrification, intensifying oxygen demand and promoting hypoxia, particularly during summer stratification when vertical oxygen replenishment was limited. These findings underscored the complex coupling between particle dynamics, primary production, and microbial nitrogen transformations, and offered important insights for hypoxia mitigation and estuarine ecosystem management.

Key words ammonia oxidation, nitrite oxidation, oxygen consumption, primary productivity, Changjiang River Estuary

Citation Zheng Zhen-Zhen, Wang Yutan, Ma Guiyi, Li Qianhui, Yang Jin-Yu Terence, Lu Anshuai, Kang Sijing, Li Moyang, Yan Xiuli, Xu Min Nina, Zheng Li-Wei, Tan Ehui, Kao Shuh-Ji. 2025. Ammonia and nitrite oxidation dynamics in the Changjiang (Yangtze) River Estuary: linking with productivity and oxygen consumption. Acta Oceanologica Sinica, 44(11): 127–140, doi: 10.1007/s13131-025-2542-9

Foundation item: The Hainan Provincial Natural Science Foundation of China under contract No. 423RC438; the Major Science and Technology Plan of Hainan Province under contract No. ZDKJ2021008; the National Natural Science Foundation of China under contract Nos 42406041, 92251306, 42266002, 41806062, and 42476032; the Open Research Fund of Guangdong Provincial Key Laboratory of Marine Disaster Prediction and Prevention under contract No. GPKLMD2023004.

*Corresponding author, E-mail: zzz@hainanu.edu.cn; ehuitan@hainanu.edu.cn

1 Introduction

Since the Industrial Revolution, anthropogenic nitrogen production has increased dramatically, reaching levels comparable to natural biological nitrogen fixation (Galloway et al., 2021). The enhanced input of reactive nitrogen has progressively accumulated in estuarine and coastal ecosystems, contributing to nutrient over-enrichment (Howarth, 2008). Elevated reactive nitrogen stimulates excessive phytoplankton growth, resulting in high primary production and increased fluxes of organic matter to deeper waters. As this organic matter settles and decomposes, microbial respiration intensifies, elevating biological oxygen demand and depleting dissolved oxygen (DO) in bottom waters (Guo et al., 2024; Wang et al., 2016).

Coastal hypoxia, typically defined as DO concentrations below 2 mg/L, has become increasingly widespread due to eutrophication and climate-driven stratification (Breitburg et al., 2018; Ma et al., 2024). It poses serious threats to aquatic ecosystems, fisheries, and biogeochemical cycling in estuarine and coastal waters worldwide (Diaz and Rosenberg, 2008). Among the processes contributing to oxygen depletion, nitrification—an obligate aerobic pathway mediated by specialized microorganisms—directly consumes DO and can significantly contribute to water-column oxygen loss, particularly under nitrogen-enriched and stratified conditions in anthropogenically impacted systems (Beman et al., 2021; Lu et al., 2020).

As a central pathway linking reduced and oxidized forms of nitrogen, nitrification comprises two sequential steps: ammonia oxidation (AO), in which ammonia is converted to nitrite (NO_2^-) by ammonia-oxidizing bacteria (AOB) or archaea (AOA); and nitrite oxidation (NO), in which NO_2^- is further oxidized to nitrate (NO_3^-) by nitrite-oxidizing bacteria (NOB) (Kuypers et al., 2018). Both steps consume oxygen, but their relative rates and environmental controls can vary widely across estuarine environments. Historically, AO was considered the rate-limiting step in nitrification, resulting in relatively less focus on NO (Tang et al., 2023). However, recent studies have shown that the relative magnitudes of ammonia oxidation rates (AOR) and nitrite oxidation rates (NOR) vary across different systems.

For instance, AOR were detectable at all euphotic zone stations of the eastern tropical South Pacific, whereas NOR were undetectable at several sites, possibly caused by the greater light sensitivity of nitrite-oxidizing processes (Peng et al., 2016). In the hypoxic zones of the Gulf of Mexico, AOR proceeded up to 30 times faster than NOR, resulting in the accumulation of NO_2^-. This decoupling likely resulted from a combination of environmental factors, with elevated bottom-water temperatures (>25℃) and substrate limitation of nitrite oxidizers being the primary contributors (Bristow et al., 2015). In contrast, NOR surpassed AOR along the southern New England coast, likely due to additional NO_2^- sources apart from AO. These included sedimentary dissimilatory NO_3^- reduction to ammonium (NH_4^+), which released NO_2^- into the overlying water column; cyanate degradation by AOA such as *Nitrosophaera gargensis*; and incomplete NO_3^- reduction by phytoplankton (Heiss and Fulweiler, 2016). In addition, cyclonic eddies in the western North Pacific were shown to enhance NOR more than AOR by selectively increasing the abundance and substrate affinity of NOB (Liu et al., 2023). In Chinese estuaries, Wan et al. (2023) reported that AOR markedly exceeded NOR in the Jiulong River Estuary, while the two rates were comparable in the Zhujiang River Estuary (ZRE) and Changjiang (Yangtze) River Estuary (CRE). Collectively, these contrasting patterns underscore the need to quantify both AOR and NOR concurrently to accurately assess nitrification-driven oxygen consumption across dynamic aquatic systems.

The CRE is one of the most eutrophic coastal systems in the world, where seasonal bottom-water hypoxia is frequently observed (Chi et al., 2020; Sheng et al., 2024; Wang et al., 2016; Zhang et al., 2019). Numerous studies have investigated the drivers of hypoxia in the CRE, highlighting the role of eutrophication, organic matter accumulation, and water column stratification (Chi et al., 2020; Liu et al., 2024; Sheng et al., 2024; Wang et al., 2016; Zhang et al., 2019). Despite these advances, most current assessments of hypoxia formation in the CRE have focused on bulk biogeochemical indicators, while the explicit contribution of nitrification remains poorly quantified. Given that nitrification is an aerobic microbial process that directly consumes oxygen and is tightly coupled with nitrogen transformations, a better understanding of its spatial dynamics and environmental controls is essential for elucidating the mechanisms underlying hypoxia development.

In this study, we simultaneously measured AOR and NOR using $^{15}NH_4^+$ and $^{15}NO_2^-$ tracer techniques in the CRE during the summer of 2022, with the aim of quantifying the contribution of nitrification to oxygen consumption. We further examined how environmental factors, such as NH_4^+ concentration, particle concentration and temperature influenced nitrification activity. Our study provided new insights into the coupled biogeochemical processes that regulate oxygen consumption and hypoxia formation in anthropogenically impacted estuarine systems.

2 Sampling and methods

2.1 *Sampling*

In this study, water samples were collected in the CRE (Fig. 1 and Table 1) from August 20 to 31, 2022, using 12-L Niskin bottles mounted on a Sea-Bird 911 conductivity-temperature-depth (CTD) rosette system. Samples for NH_4^+, NO_2^-, and NO_3^- analyses were filtered through 0.22 μm polycarbonate membranes to remove active cells

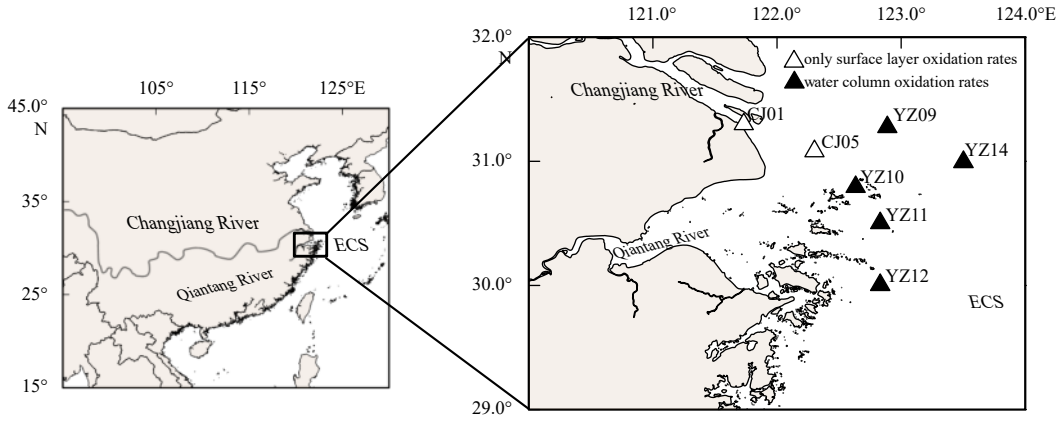

Fig. 1. Map of sampling sites located off the Changjiang River Estuary (CRE) in the East China Sea (ECS) shelf. Solid triangles mark locations where water column oxidation rates were measured, whereas hollow triangles denote sites where only surface oxidation rates were recorded.

and minimize post-sampling microbial activity that could alter nutrient concentrations. The filtrates were collected into 50 mL centrifuge tubes (BD Falcon) and stored for subsequent analysis. Total suspended matter (TSM) samples were collected by filtering 300–500 mL of water through pre-combusted (450℃ for 4 h) and pre-weighed glass microfiber filters (GF/F). After filtration, filters were folded and wrapped in pre-combusted aluminum foil (450℃ for 4 h). Nutrient and TSM samples were stored at −20℃ until analysis.

2.2 *Ammonia and nitrite oxidation rate incubation experiments*

Oxidation rate incubations were conducted using an artificial isotope addition method. For each sampling depth, six replicate water samples (150 mL each) were collected in high-density polyethylene (HDPE) bottles. Three replicates were used for AOR incubations, and the remaining three for NOR incubations. For AOR, $^{15}NH_4^+$ was added, while $^{15}NO_2^-$ was introduced for NOR incubations. To minimize artificial stimulation of microbial activity, tracer additions were generally recommended to be approximately 10% of ambient substrate concentrations. However, because *in situ* nutrient concentrations were not known prior to sampling, we referred to previously reported levels in the CRE, where NH_4^+ typically ranged from 0.5 μmol/L to 2.0 μmol/L and NO_2^- from 0.05 μmol/L to 1.0 μmol/L (Hsiao et al., 2014). Accordingly, tracer concentrations of 0.2 μmol/L $^{15}NH_4^+$ and 0.06 μmol/L $^{15}NO_2^-$ were used in the incubations.

The samples were then incubated at *in situ* temperature, and 50 mL subsamples were withdrawn from each incubation bottle at 0 and about 6 h, then filtered through a 0.22 μm polycarbonate membrane. The filtrates were collected and stored at −20℃ for subsequent isotopic analysis.

2.3 *Hydrographical chemical analyses*

Environmental parameters, including salinity, temperature, depth, photosynthetically active radiation (PAR), DO, pH, and fluorescence were measured using a CTD sensor package. Ammonium concentrations were analyzed via the indophenol blue spectrophotometric method, with a detection limit of 0.3 μmol/L. For samples with NH_4^+ concentrations below this threshold, solid-phase extraction followed by fluorescence detection was employed, which achieved a detection limit of 2.2 nmol/L. NO_3^- and NO_2^- concentrations were determined using an AA3 Auto-Analyzer with a detection limit of 0.01 μmol/L. TSM concentrations were quantified by the weight difference method.

2.4 *Measurement of ammonia and nitrite oxidation rates*

For AOR measurements, the $\delta^{15}N\text{-}NO_x^-$ was determined using the denitrifier method (Sigman et al., 2001). The isotopic composition of bacteria-produced N_2O was measured by a Gasbench (Thermo Fisher) connected to an Isotope Ratio Mass Spectrometer (Thermo Delta V Advantage). For NOR measurements, preexisting NO_2^- was removed by adding sulfamic acid to the sample and allowing it to react for 1 h. Subsequently, sodium hydroxide was added to adjust the pH to neutrality (Granger and Sigman, 2009). The $\delta^{15}N\text{-}NO_3^-$ was then measured using the denitrifier method.

The rates were calculated by the following Eq. (1):

$$\text{Rate} = \frac{\Delta^{15}N}{f_S^{15} \times t}, \tag{1}$$

where Rate refers to AOR or NOR, t is the incubation time, $\Delta^{15}N$ represents the change in concentration in the production pool (NO_x^- for AOR and NO_3^- for NOR) between the start and end of the incubation, and f_S^{15} is the fraction of substrate (NH_4^+ for AOR and NO_2^- for NOR) labeled with ^{15}N at the start of the incubation.

Table 1. Environmental factors and nitrification rates at sampling sites

Station	Latitude/ °N	Longitude/ °E	Depth/ m	AOR/ (nmol·L^{-1}·d^{-1})	NOR/ (nmol·L^{-1}·d^{-1})	TSM/ (mg·L^{-1})	Temperature/ ℃	Salinity	NH_4^+/ (μmol·L^{-1})	NO_2^-/ (μmol·L^{-1})	NO_3^-/ (μmol·L^{-1})	Chl *a*- from CTD/(μg·L^{-1})	DO- from CTD/(μmol·L^{-1})	pH- from CTD
CJ01	31.31	121.73	3	1 609.0 ± 31.3	479.9 ± 14.7	50.75	32.20	0.44	1.7	0.29	153.00	2.69	207.50	7.92
CJ05	31.08	122.30	3	174.0 ± 7.2	314.6 ± 0.5	37.50	28.77	23.64	0.3	1.45	56.44	3.72	189.06	7.92
YZ09	31.28	122.89	3	0.5 ± 0.02	3.6 ± 0.2	1.60	26.41	28.89	1.7	0.36	7.84	50.74	403.44	8.56
			14	144.9 ± 7.0	45.4 ± 1.9	1.65	20.65	33.93	0.3	0.04	15.00	1.06	150.94	7.99
			60	1 109.7 ± 69.4	247.0 ± 22.1	3.45	20.61	34.19	1.1	0.24	17.91	1.42	47.50	7.87
YZ10	30.79	122.63	8	283.6 ± 7.3	4.4 ± 0.1	4.85	23.88	31.46	0.2	0.77	15.22	6.86	185.63	7.99
			14	389.4 ± 18.0	5.4 ± 0.9	2.90	23.62	32.06	0.5	0.70	16.37	0.14	140.94	7.91
			22	496.2 ± 16.3	649.9 ± 19.0	11.60	22.95	32.78	0.2	1.18	17.40	0.47	119.69	7.92
YZ11	30.50	122.83	3	4.7 ± 0.2	0.01 ± 0.00	1.65	27.64	32.63	0.6	0.12	1.08	2.54	199.06	8.17
			8	14.6 ± 0.2	6.4 ± 1.5	1.95	26.83	32.85	0.8	0.72	1.95	3.28	201.25	8.11
			14	299.6 ± 20.9	110.8 ± 2.2	0.90	24.57	33.73	0.7	1.07	4.86	0.31	123.44	7.91
			24	304.1 ± 21.3	264.2 ± 2.2	4.95	20.99	34.21	0.1	0.54	9.61	0.39	96.56	7.93
			35	867.7 ± 15.0	224.5 ± 3.3	37.20	20.95	34.23	0.4	0.38	9.38	0.39	89.38	7.94
YZ12	30.00	122.83	3	0.3 ± 0.1	1.0 ± 0.2	3.80	27.88	31.19	0.7	0.03	0.38	14.35	265.31	8.31
			12	52.3 ± 4.2	20.0 ± 0.1	0.85	25.62	32.77	1.0	0.37	2.33	6.33	234.06	8.15
			20	120.9 ± 4.6	75.8 ± 3.4	1.50	22.04	33.81	0.1	0.27	8.86	0.85	132.81	7.90
			30	196.8 ± 10.9	309.0 ± 23.3	5.35	20.38	34.11	0.05	0.34	13.64	0.85	82.81	7.89
			40	915.3 ± 9.4	410.0 ± 4.3	16.10	19.37	34.27	0.6	0.46	17.54	0.85	65.31	7.87
YZ14	31.00	123.50	18	0.5 ± 0.1	0.06 ± 0.01	1.20	27.30	33.68	0.4	0.02	0.10	0.64	202.81	8.15
			25	65.9 ± 2.7	9.2 ± 1.7	1.70	24.46	33.92	0.2	0.34	1.90	6.09	186.25	8.08
			35	166.9 ± 10.9	188.9 ± 6.9	3.70	20.52	34.25	0.3	0.32	8.19	0.19	91.88	7.90
			48	265.8 ± 23.0	240.5 ± 12.3	12.20	19.97	34.30	0.2	0.21	15.18	0.11	88.44	7.93

3 Results

3.1 *Spatial distribution of environmental parameters and nitrification rates in surface waters*

Surface water temperatures ranged from 24.2℃ to 32.2℃, with the highest values recorded near the estuary and the lowest in the center of the sampling area (Fig. 2a). Salinity varied from 0.4 to 33.7, generally increasing with distance offshore (Fig. 2b). The maximum dissolved inorganic nitrogen (DIN, including NH_4^+, NO_2^-, NO_3^-) concentration was observed at Station CJ01 near the river mouth, reaching 155.0 μmol/L, but decreased to less than 1 μmol/L further offshore (Fig. 2c). NH_4^+ concentrations ranged from 0.2 μmol/L to 1.7 μmol/L, with the highest levels detected at stations YZ09 and CJ01 (Fig. 2d). The concentrations of NO_2^- and NO_3^- varied from 0.01 μmol/L to 1.8 μmol/L and 0.1 μmol/L to 153.0 μmol/L, respectively, exhibiting a spatial pattern consistent with that of DIN, with higher concentrations nearshore and decreasing offshore (Figs 2e and f). Near the river mouth, NO_3^- was the dominant form of DIN, accounting for 99% of the total. In contrast, offshore waters were dominated by NH_4^+, which constituted more than 76% of the DIN pool. Chlorophyll *a* (Chl *a*) concentrations ranged from 0.09 μg/L to 50.74 μg/L, exhibiting a spatial distribution like that of NH_4^+, with the highest values observed at Station YZ09 in the northern region (Fig. 2g). The concentration of TSM varied from 1.6 mg/L to 50.8 mg/L, which showed a trend of higher concentrations near the estuary and lower levels offshore (Fig. 2h). Dissolved oxygen concentrations varied between 189 μmol/L and 403 μmol/L, displaying spatial patterns consistent with NH_4^+ and Chl *a* concentration (Fig. 2i).

In surface waters, AOR ranged from 0.3 nmol/(L·d) to 1 609 nmol/(L·d), while NOR ranged from 0.01 nmol/(L·d) to 480 nmol/(L·d). On average, AOR [357 nmol/(L·d)] was higher than NOR [160 nmol/(L·d)] across the study area (Fig. 3), which highlighted the dominant role of AO in surface-layer nitrification. Notably, the highest nitrification rates were observed at the river mouth Station CJ01 (Fig. 3), where NH_4^+ and TSM concentrations were also elevated (Figs 2c and h). These findings underscored the pronounced spatial heterogeneity of nitrification in the estuarine environment, with microbial oxidation processes most active near the river mouth, where substrates and suspended particles provided favorable conditions for nitrifying microorganisms.

3.2 *Vertical distribution of environmental parameters and nitrification rates*

At the research stations, temperature decreased with depth, while salinity showed the opposite pattern, starting low at the surface and increasing to approximately 34 at the bottom. Thermoclines and haloclines were found at similar depths at each station. The euphotic zone depth—defined as the depth where light intensity is 1% of surface levels (grey dashed line in Figs 4a1, b1, c1, d1, and

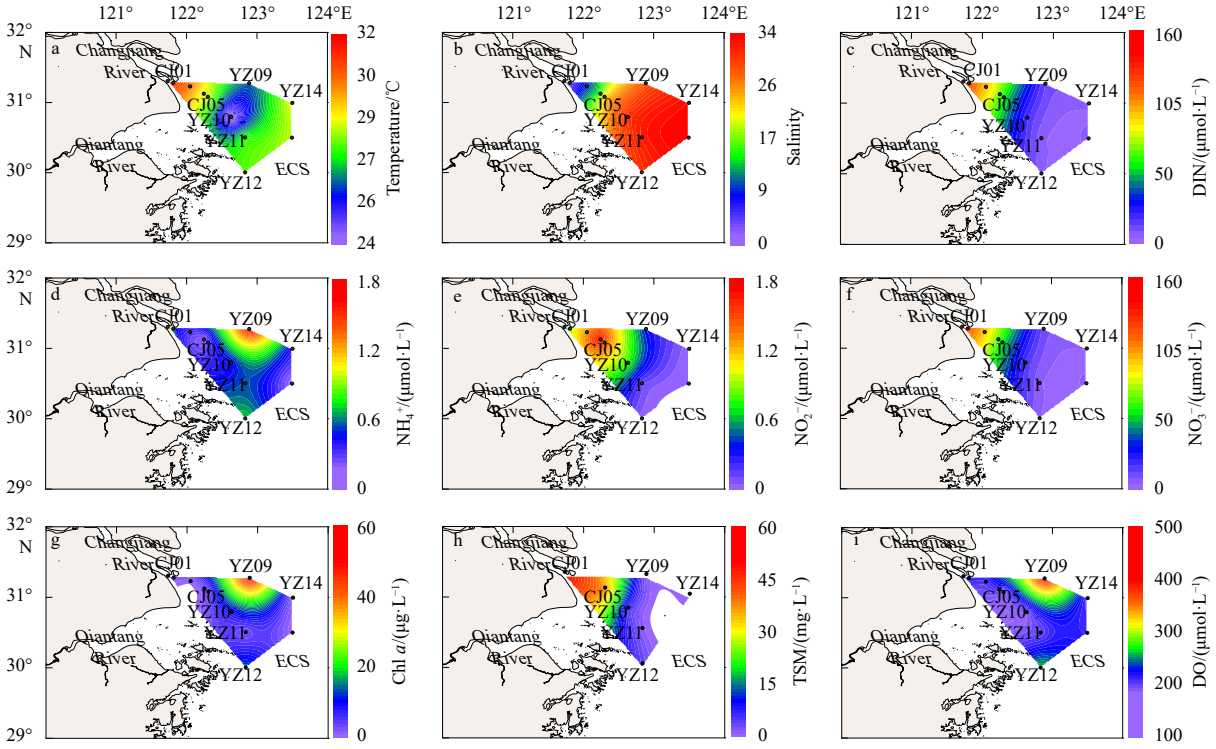

Fig. 2. Surface distribution of key environmental parameters in the Changjiang River Estuary (CRE). a. temperature measured by CTD; b. salinity measured by CTD; c. concentration of dissolved inorganic nitrogen (DIN); d. ammonium (NH_4^+); e. nitrite (NO_2^-); f. nitrate (NO_3^-); g. chlorophyll *a* (Chl *a*) measured by CTD; h. total suspended matter (TSM); i. dissolved oxygen (DO) measured by CTD.

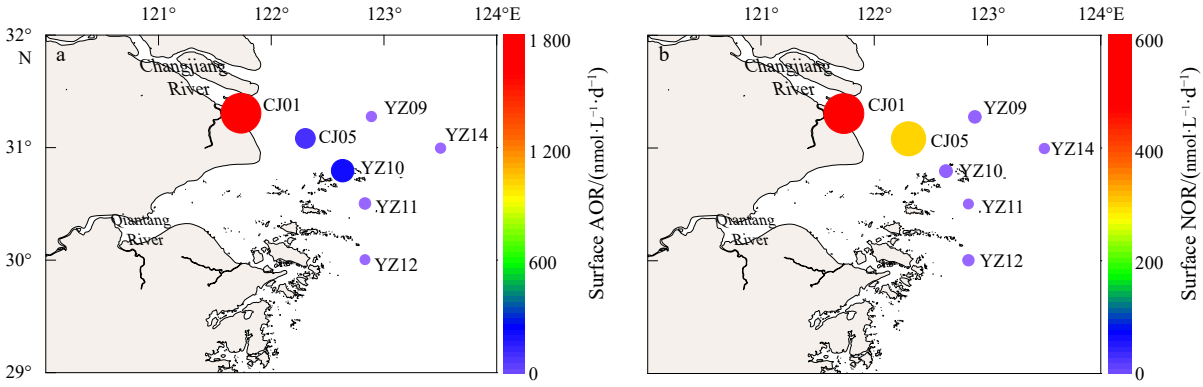

Fig. 3. Distribution of ammonium oxidation rates (AOR) (a) and nitrite oxidation rates (NOR) (b) in surface waters of the Changjiang River Estuary (CRE).

e1)—deepened as the distance from shore increased, ranging from less than 10 m at Stations YZ09, YZ10, and YZ12, to over 35 m at Station YZ14. High Chl *a* concentration was observed within the euphotic zone, but dropped sharply below the halocline (Figs 4a1, b1, c1, d1, and e1).

DO concentrations decreased with depth at all stations, reaching suboxic to hypoxic levels at the bottom (48–120 μmol/L). Hypoxia was observed at the bottom of stations YZ09 and YZ12, indicating a significant depletion of DO in these areas. TSM concentrations ranged from 0.9 mg/L to 37.2 mg/L, increasing with depth and reaching maximum levels at the bottom of Station YZ11 (Figs 4a2, b2, c2, d2, and e2).

Ammonium concentrations ranged from 0.1 μmol/L to 1.7 μmol/L, while NO_3^- and NO_2^- concentrations varied from 0.1 μmol/L to 20.9 μmol/L and 0.02 μmol/L to 1.2 μmol/L, respectively, showing a pattern of lower concentrations at the surface and higher concentrations at the bottom. NH_4^+ and NO_2^- concentrations were significantly lower compared to NO_3^-. Elevated NO_2^- concentrations were particularly notable near the euphotic zone (Figs 4a3, b3, c3, d3, and e3).

AOR ranged from 0.3 nmol/(L·d) to 1 110 nmol/(L·d) and NOR from 0.01 nmol/(L·d) to 650 nmol/(L·d) in the vertical profiles. Both rates were lower at the surface and increased with depth, reaching their highest values near the bottom. AOR were consistently higher than NOR at most stations, which highlighted the dominance of AO throughout the water column (Figs 4a4, b4, c4, d4, and e4).

4 Discussion

4.1 *The relationship between nitrification rates and environmental factors*

In our study, the AOR were on average about twice those of NOR across all sampled stations and depths. This contrasted with the "comparable rates" reported by Wan et al. (2023), who observed similar magnitudes of AOR and NOR during springtime in the CRE. This discrepancy likely reflected seasonal differences in water-column stratification. Wan et al. (2023) sampled under relatively weakly stratified and well-oxygenated conditions, whereas our summer sampling captured periods of pronounced stratification and bottom-water hypoxia. Such conditions tend to decouple AO and NO processes, partly because nitrite-oxidizing microorganisms are more sensitive to oxygen limitation than ammonia oxidizers (Guisasola et al., 2005).

Despite differences in their absolute rates, we observed a significant positive correlation between AOR and NOR (Fig. 5), indicating that the two processes responded similarly to spatial environmental gradients. Both AOR and NOR declined with increasing distance offshore and exhibited depth-dependent patterns, with lower values in surface waters and higher rates near the bottom (Figs 3 and 4). This pattern was shaped by multiple environmental drivers, including substrate availability (e.g., NH_4^+ and NO_2^- concentrations), suspended particulate matter, temperature, pH, salinity, and DO (Figs 6 and 7).

4.1.1 *Ammonia oxidation and environmental factors*

Photoinhibition exerted a pronounced suppression on AOR in surface waters (Fig. 6, yellow circles), where elevated NH_4^+ concentrations did not result in higher AOR (Fig. 6a). This phenomenon, widely documented in previous studies (e.g., Ward, 2005), is not discussed in detail here. Below the photic zone, however, NH_4^+ emerged as the dominant driver of AOR across depths in the YRE, where concentrations ranged from 0.05 μmol/L to 1.66 μmol/L. AOR exhibited a strong positive correlation with NH_4^+ concentrations (r = 0.9, p < 0.001; Fig. 6a), a relationship also widely reported in both nearshore and offshore environments (Peng et al., 2016; Wang et al., 2018; Zheng et al., 2017). Stations with elevated NH_4^+, particularly in nearshore regions, exhibited the highest AOR, indicating that increased substrate availability directly stimulated microbial AO activity. Interestingly, stations CJ01 and CJ05, despite both being located relatively close to shore, exhibited markedly different AOR. CJ01 showed AOR close to the upper bound, whereas CJ05

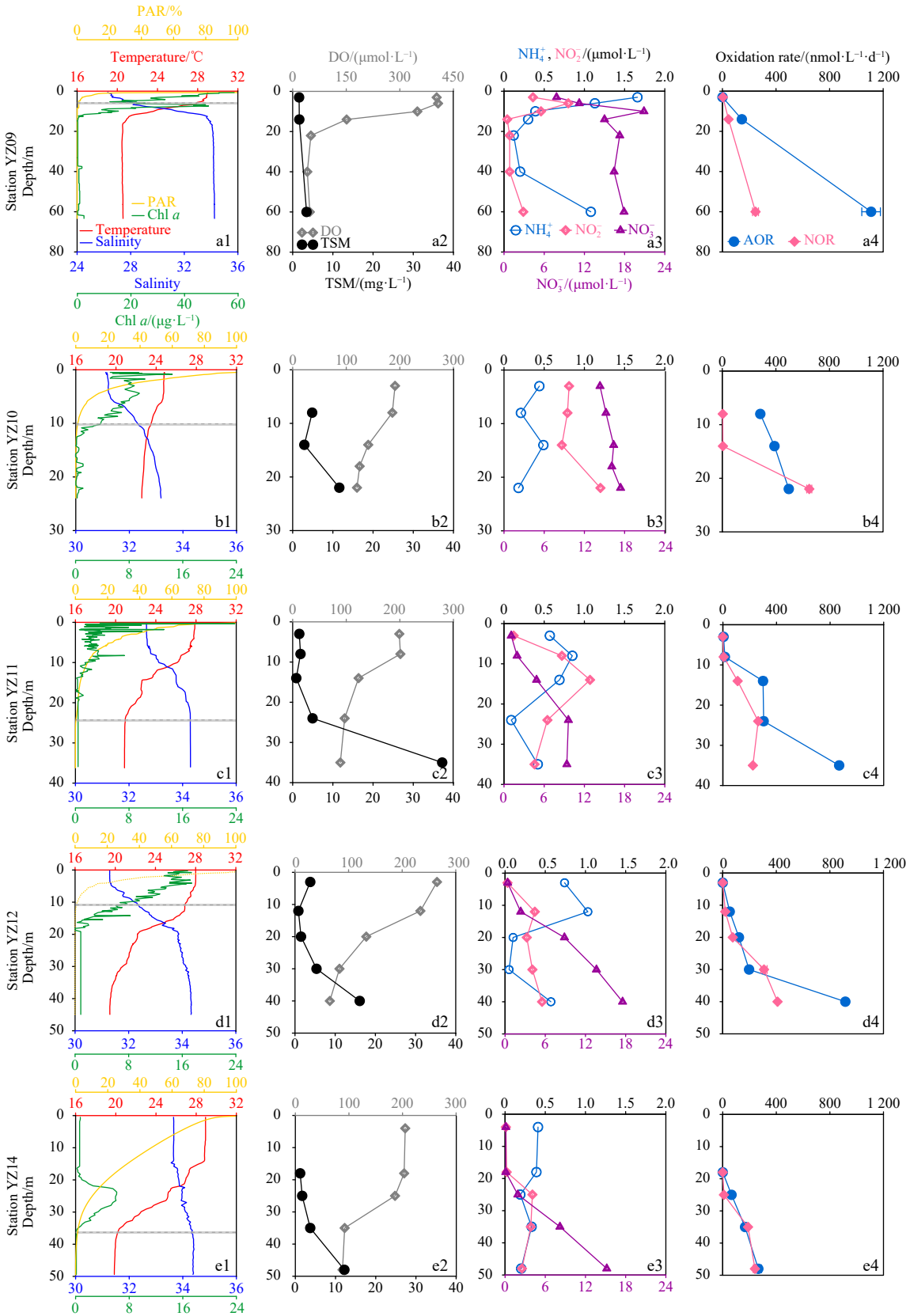

Fig. 4. Vertical distributions of temperature, salinity, photosynthetically active radiation (PAR), and chlorophyll *a* (Chl *a*) concentration (a1, b1, c1, d1, and e1); dissolved oxygen (DO) and total suspended matter (TSM) concentrations (a2, b2, c2, d2, and e2); the concentrations of ammonium (NH_4^+), nitrite (NO_2^-) and nitrate (NO_3^-) (a3, b3, c3, d3, and e3); ammonia oxidation rates (AOR) and nitrite oxidation rates (NOR) (a4, b4, c4, d4, and e4). The grey dashed lines represent the depths at which light intensity is 1% of surface levels.

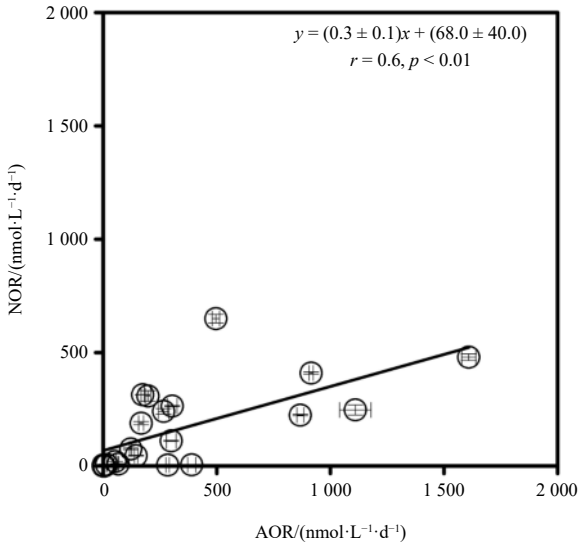

Fig. 5. Relationship between ammonia oxidation rates (AOR) and nitrite oxidation rates (NOR) in the study area.

consistently displayed some of the lowest values observed. This divergence could be attributed to stark differences in NH_4^+ concentrations between the two stations, reinforcing the central role of substrate supply in modulating AOR (Fig. 6a).

Microbial community composition also modulates AOR responses to NH_4^+ availability. Previous studies have revealed distinct differences in ammonia-oxidizing microbial communities between the inner and outer estuary, with AOB dominating the inner estuary and AOA prevailing in the outer estuary (Dai et al., 2022). This community shift is associated with pronounced differences in the half-saturation constants (K_m) for NH_4^+ between AOA and AOB. Studies in both pure cultures and field conditions showed that K_m values for AOB ranged from 28 μmol/L to 50 000 μmol/L, whereas K_m values for AOA were much lower, ranging from 30 nmol/L to 150 nmol/L (Kits et al., 2017; Martens-Habbena et al., 2009; Zheng et al., 2020). In our study area, NH_4^+ concentrations at most depths remained below the saturation level for AOA and well below that for AOB, leading to increased AOR with rising NH_4^+ concentrations.

Although AO is strictly aerobic, our results revealed a negative correlation between AOR and DO concentrations (Fig. 6b). Oxygen concentrations in the study area ranged from 41.3 μmol/L to 406.9 μmol/L, which were well above the oxygen-limitation thresholds for AO. Previous studies have demonstrated that both AOA and AOB are capable of functioning effectively under extremely low oxygen conditions. For example, AO in the South Pacific exhibited a K_m for oxygen as low as (0.3 ± 0.1) μmol/L (Bristow et al., 2016), and pure cultures of AOA and AOB showed oxygen K_m values ranging from 2.0–3.9 μmol/L and 15.6–186.0 μmol/L, respectively (Park et al., 2010). Therefore, the observed inverse relationship likely reflected enhanced AO activity contributing to oxygen consump-

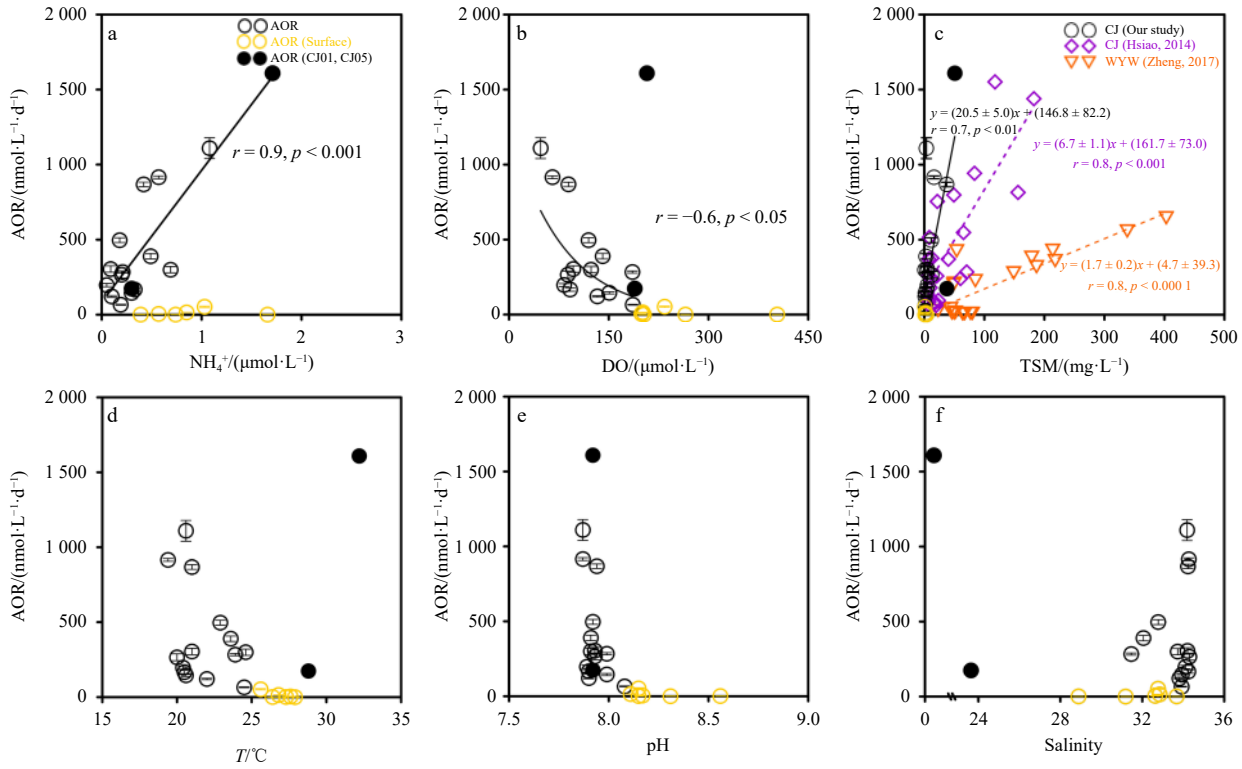

Fig. 6. Correlations between ammonia oxidation rates (AOR) and various environmental factors. a. ammonium (NH_4^+) concentration; b. dissolved oxygen (DO) concentration; c. total suspended matter (TSM) concentration; d. temperature; e. pH; f. salinity. The yellow hollow cycles represent the AOR at the surface layers with light suppression, and the black solid circles represent the stations near the estuary where turbidity was high.

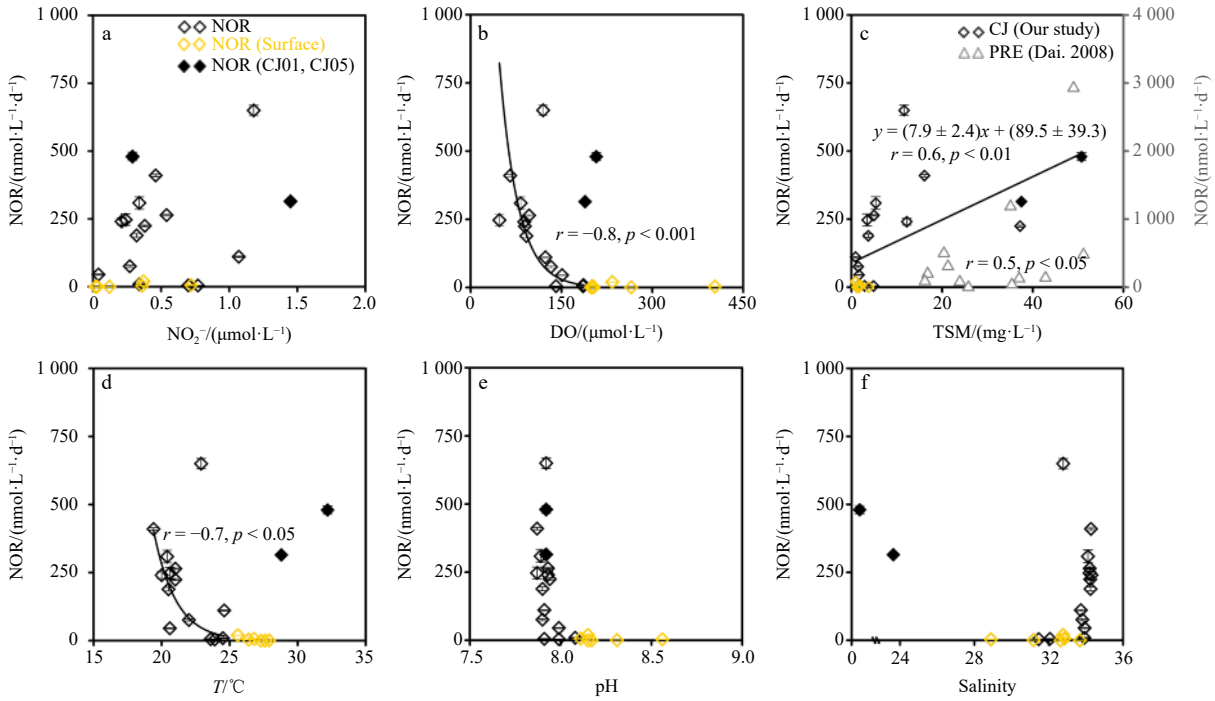

Fig. 7. Correlations between nitrite oxidation rates (NOR) and various environmental factors. a. nitrite (NO_2^-) concentration; b. dissolved oxygen (DO) concentration; c. total suspended matter (TSM) concentration; d. temperature; e. pH; f. salinity. Yellow hollow diamonds denote NOR in surface layers under light suppression, and black solid diamonds represent the stations near the estuary where turbidity was high.

tion in stratified and hypoxic bottom waters, particularly during the summer sampling period.

In addition to NH_4^+ concentration, particulate matter also played a significant role in regulating AOR, as indicated by their positive correlation with TSM (Fig. 6c, r = 0.7, p < 0.01). This pattern was consistent with previous observations from the CRE (Hsiao et al., 2014) as well as other high-turbidity systems such as San Francisco Bay and Wuyuan Bay in southern China (Damashek et al., 2016; Zheng et al., 2017). Suspended particles may enhance AOR through two mechanisms: (1) providing surface area for microbial colonization and (2) releasing NH_4^+ via organic matter mineralization (Xia et al., 2009). Notably, although TSM concentrations in the YRE were lower (<55 mg/L) than those in Wuyuan Bay (which reached up to 400 mg/L), AOR in our study reached much higher values [up to 1 600 nmol/(L·d) compared with <600 nmol/(L·d)] (Fig. 6c), suggesting that smaller particles with higher specific surface area may compensate for lower mass loading and still sustain elevated AO activity. This may also explain why AOR remained high despite a nearly fivefold decline in riverine TSM since the summer of 2011 (Hsiao et al., 2014), driven by damming and other anthropogenic activities.

Temperature is another important environmental factor influencing AO, primarily through its effect on the enzymatic activity of ammonia-oxidizing microorganisms (Taylor and Mellbye, 2022; Zheng et al., 2017). In our study, higher rates were typically observed in cooler regions, except at CJ01—the innermost nearshore station—where elevated rates coincided with high temperature (Fig. 6d). This inverse relationship may be attributed to the fact that, under substrate-limited conditions, the optimal temperature for AO activity was lower than that in substrate-sufficient conditions (Zheng et al., 2020). This interpretation is consistent with the generally low NH_4^+ concentrations observed across most of our sampling sites. The contrasting pattern at CJ01 further supported this mechanism. At this site, where both turbidity and NH_4^+ concentrations were highest, AOR remained elevated even under warmer conditions. This was in line with previous findings from pure culture and field studies, which showed that AOR—and the growth of AOA—increased with temperature under substrate-saturated conditions, typically reaching optima between 25℃ and 34℃ (Qin et al., 2014; Zheng et al., 2020). Moreover, a coastal-to-offshore transect study revealed that substrate enrichment could shift the thermal optimum of AO microbes upward when background substrate levels were insufficient (Zheng et al., 2020). Taken together, our results suggested that substrate availability not only regulates the magnitude of AOR but may also modulate its temperature sensitivity. However, an alternative or complementary explanation cannot be ruled out. Many of the low-temperature observations corresponded to bottom waters, which were typically characterized by higher turbidity. As discussed earlier, AOR were positively correlated with TSM. Therefore, the elevated AOR observed at cooler depths may reflect, at least in part, the influence of increased particle concentrations. Disentangling the effects of these co-vary-

ing factors would require controlled incubations or targeted molecular analyses of ammonia-oxidizing communities.

In addition to temperature, pH is another factor influencing AO by affecting microbial enzymatic activity and substrate speciation. In our study, pH varied more widely at the surface (7.9–8.6) but was relatively stable (7.9–8.1) at other depths. AOR did not exhibit a clear correlation with pH (Fig. 6e), suggesting that AOR in the CRE were not strongly influenced by pH fluctuations. This finding contrasted with results from many field studies. Acidification experiments in marine systems reported reduced AOR under low pH (Beman et al., 2011; Zhou et al., 2023).

Salinity influences both the biological activity and community structure of ammonia-oxidizing microorganisms (Wei and Lin, 2021). Our results showed that along the horizontal gradient, higher AOR occurred in low-salinity areas, while along the vertical profile, higher AOR were found in deeper, high-salinity layers (Fig. 6f). This distribution pattern may reflect the combined effects of salinity and other factors, such as light, nutrient availability, and particulate concentrations.

4.1.2 *Nitrite oxidation and environmental factors*

Nitrite oxidation rates ranged from 0 nmol/(L·d) to 650 nmol/(L·d) across the study area, with elevated values predominantly observed at nearshore stations and in the bottom waters of offshore sites. Consistent with AOR, NOR was strongly suppressed in surface waters due to photoinhibition, resulting in low surface rates. However, unlike AOR, which exhibited a clear positive correlation with its substrate (NH_4^+), NOR showed no significant correlation with ambient NO_2^- concentrations (Fig. 7a). This lack of correlation may stem from the fact that NO_2^- produced *in situ* by AO directly fueled the NO process, rather than relying solely on ambient NO_2^-. The significant positive correlation between AOR and NOR ($r = 0.6$, $p < 0.01$; Fig. 5) supported this coupling between the two processes. NOR also displayed negative correlations with DO and positive correlations with TSM (Figs 7b and c), indicating that both processes responded to shared biogeochemical gradients in the estuarine system.

NO is an oxygen-dependent process, in which oxygen serves as the terminal electron acceptor. If DO was limiting, we would expect a positive correlation between NOR and DO concentrations. However, in our study, NOR and DO exhibited a significant negative correlation (Fig. 7b), indicating that oxygen concentrations in the CRE were well above the threshold required for NO. This suggested that DO was not a limiting factor for NOR in our system. This interpretation was consistent with the high oxygen affinity of NOB, which were reported the K_m value for oxygen below 1 μmol/L (Bristow et al., 2016). In such cases, NO can proceed efficiently even at very low oxygen concentrations, reinforcing the idea that the process is rarely oxygen-limited in natural environments. Indeed, a global synthesis by Tang et al. (2023) showed that NOR often peaked within oxygen minimum zones, including regions where DO fell below detection limits. Similarly, Sun et al. (2023) documented declining NOR with increasing oxygen, further supporting the notion that NO is active in low-oxygen zones. Taken together, these findings—and our own observations—suggested that NO not only tolerated low-oxygen conditions but also contributed to oxygen depletion in estuarine bottom waters. These findings highlighted NO as a potentially important but underappreciated driver of coastal hypoxia.

Researchers such as Füssel et al. (2012) have observed that nitrite-oxidizing microorganisms tend to attach to particles in nearshore waters. However, in our study area, the positive correlation between NOR and TSM was weaker ($r = 0.60$, $p < 0.01$, Fig. 7c) compared to AOR ($r = 0.7$, $p < 0.01$, Fig. 6c). Additionally, a study in the ZRE found no significant relationship between NOR and TSM (Dai et al., 2008; Fig. 7c). This suggested that AO organisms may adhere more readily to particles than NO organisms, possibly because AO organisms have a smaller cell diameter and larger specific surface area, which allow particles to adsorb more biomass (Pachiadaki et al., 2017).

Pure culture and field-based temperature manipulation experiments showed that, under substrate-saturated conditions, NOB typically exhibit optimal activity at temperatures between 22℃ and 39℃ (Ehrich et al., 1995; Nowka et al., 2015; Schaefer and Hollibaugh, 2017). However, in our study, NOR decreased with increasing temperature across the observed range (19.4–32.2℃; Fig. 7d), a pattern similar to that of AOR. This inverse relationship suggested that, like AO, NO in the CRE was likely substrate-limited, such that higher temperatures did not enhance—and may even suppress—enzymatic activity under nutrient-scarce conditions. In addition, this pattern may reflect co-varying environmental factors. Higher NOR values tended to occur in cooler, deeper waters with elevated particle concentrations, whereas surface layers with stronger light exposure and higher temperatures may experience photoinhibition of nitrite oxidizers, further limiting NOR in those zones.

As for pH, our results showed no clear correlation between pH and NOR (Fig. 7e), mirroring the weak pH sensitivity of AOR observed in this study. Although previous studies have reported inhibitory effects of high pH on NOB—particularly in surface waters influenced by phytoplankton-driven photosynthetic alkalinization (Heiss and Fulweiler, 2016)—our data suggested that pH variability within the CRE was not a dominant factor regulating NO. Instead, other environmental drivers such as substrate availability, light, and particle load likely played more critical roles.

Consistent with AOR, higher NOR values were observed in both the low salinity regions of the estuary and the high salinity near-bottom waters (Fig. 7f), primarily due to high turbidity and low light intensity in these regions.

While these results provided valuable insights into the environmental controls on nitrification during summer stratification, they were based on a single sampling campaign and may not reflect broader temporal variability. This limited our ability to extrapolate the observed patterns to other seasons or years. Previous studies in the CRE and adjacent waters have documented pronounced seasonal differences in nitrification dynamics across both the water column and sediments. In the water column, Wang et al. (2018) observed that summer conditions with strong stratification and localized NH_4^+ regeneration led to higher nitrification rates in nearshore bottom waters, whereas in winter, reduced stratification and enhanced vertical mixing supported higher nitrification rates offshore and more evenly distributed throughout the water column. Hou et al. (2025) further highlighted the role of light inhibition and organic matter regeneration in shaping these seasonal patterns. Their results showed that summer nitrification rates peaked in bottom layers of high-productivity and turbidity zones, where *in situ* mineralization supplied abundant NH_4^+, while strong light in surface waters suppressed nitrification and favored phytoplankton NH_4^+ uptake. Gao et al. (2018) reported significantly higher nitrification rates in sediments during summer than winter, driven by elevated temperatures and greater NH_4^+ availability, along with shifts in microbial community composition—higher AOB diversity and increased AOA abundance in summer. Collectively, these studies demonstrated that seasonal variations in temperature, stratification, NH_4^+ regeneration, and light conditions created distinct vertical niches for nitrification.

4.2 *The influence of primary productivity on bottom water nitrification and oxygen dynamics*

We integrated Chl *a* concentration (IChl *a*) within the euphotic zone (where light intensity exceeds 1% of surface levels) to assess how primary productivity may impact AOR in the bottom water. Our analysis showed that as IChl *a* increased, AOR in the bottom layer also increased (Fig. 8a), suggesting a potential link between euphotic zone productivity and AOR in deeper water. In addition, the positive association between IChl *a* and bottom-water NH_4^+ concentrations (Fig. 8b) suggested that primary production in the euphotic zone contributed to NH_4^+ enrichment at depth, which in turn fueled nitrifying microbial activity.

This interaction between surface productivity and bottom-water AOR also highlighted a potential feedback mechanism whereby surface-driven nutrient cycling can influence oxygen dynamics in deeper waters. The enhanced AOR, driven by high NH_4^+ availability, could lead to significant oxygen consumption, especially in stratified water bodies where oxygen replenishment was limited. Hypoxia in this region typically begins developing in early summer, reaching its peak intensity in August. Our field observations from August 20th to 31st recorded bottom layer oxygen concentrations ranging from 47.5 μmol/L to 112 μmol/L, indicative of hypoxic or sub-hypoxic conditions.

To evaluate the oxygen cost of this coupled process, we used stoichiometric equations (Eqs (2)–(5)) to estimate oxygen consumption during organic matter mineralization. We hypothesized that the NH_4^+ utilized in the AO process within the bottom water originated primarily from the mineralization of organic matter (Yan et al., 2017).

$$C_{106}H_{175}O_{42}N_{16}P + 118O_2 \rightarrow 106CO_2 + 16NH_4^+ + HPO_4^{2-} + 48H_2O + 14OH^-, \quad (2)$$

$$2NH_4^+ + 3O_2 \rightarrow 2NO_2^- + 2H_2O + 4H^+, \quad (3)$$

$$2NO_2^- + O_2 \rightarrow 2NO_3^-, \quad (4)$$

$$C_{106}H_{175}O_{42}N_{16}P + 150O_2 \rightarrow 106CO_2 + 16NO_3^- + HPO_4^{2-} + 78H_2O + 18H^+. \quad (5)$$

Base on Eqs (2)–(5), the complete oxidation of one mole of organic matter to NO_3^- consumes 150 mol O_2—118 mol for organic matter mineralization to NH_4^+, and 32 mol for AO and NO. Thus, nitrification accounts for approximately 21% of the total oxygen consumption associated with this transformation. Based on our field AOR

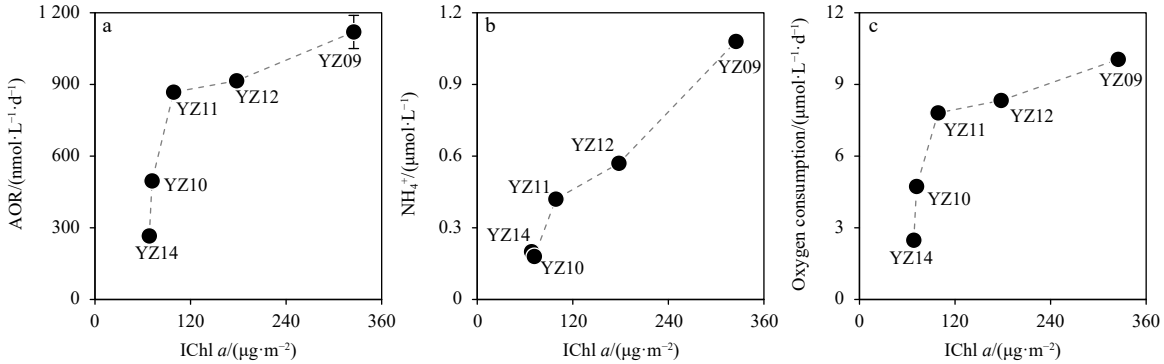

Fig. 8. Relationship between the integral of chlorophyll *a* concentration (IChl *a*) and ammonia oxidation rates (AOR) (a), ammonium (NH_4^+) concentration (b) and oxygen consumption in the bottom layer (c).

and NOR estimates, the oxygen consumption attributable to these processes ranged from 2.47 μmol/(L·d) to 10.17 μmol/(L·d). It should be noted that our calculations may underestimate the total oxygen consumption rate—by not accounting for the oxygen required for the mineralization of NH_4^+ that was not oxidized to NO_2^-.

We further observed a positive correlation between IChl*a* and bottom-water oxygen consumption (Fig. 8c), reinforcing the notion that surface productivity indirectly contributed to deep-water oxygen loss. Although our estimates were based on limited stations and do not account for physical processes such as endmember mixing or lateral advection, the trends pointed to organic matter mineralization, including nitrification, as important drivers of summer hypoxia in the CRE.

In addition, high riverine nitrogen inputs enhanced surface phytoplankton production, increasing particulate nitrogen (PN) flux to depth. These particles underwent remineralization, releasing NH_4^+ that fueled AOR and NOR —both of which consumed oxygen. Under strong summer stratification, restricted vertical mixing further impeded oxygen resupply, compounding hypoxia in bottom waters (Fig. 9).

Overall, our results highlighted a strong vertical coupling between surface water productivity, bottom-water nitrification activity, and oxygen depletion. Organic particles exported from productive surface layers not only served as a source of NH_4^+ via remineralization but also provided microhabitats for particle-associated ammonia oxidizers (Fig. 9). This mechanistic linkage underscored how surface-driven productivity can indirectly drive subsurface oxygen depletion via microbial nitrogen transformations.

5 Conclusions

This study provided new insights into the microbial processes driving oxygen consumption in the CRE during summer hypoxia. By simultaneously quantifying AOR and NOR using ^{15}N tracer techniques, we demonstrated that AOR generally exceeded NOR across depths and stations. These findings highlighted the predominance of AO in this estuary and the importance of considering both nitrification steps in oxygen budget assessments. We also showed that AOR was significantly enhanced by NH_4^+ availability and TSM, indicating a strong link between particle-associated microhabitats and microbial nitrifier activity. Furthermore, a robust relationship between surface Chl *a* and bottom-water AOR supported the concept of vertical coupling: high surface productivity enhanced organic matter export and NH_4^+ regeneration, which fueled deep nitrification and associated oxygen consumption. Estimated oxygen consumption from nitrification constitutes a significant component of total biological oxygen demand in the CRE.

These findings provided mechanistic support for the feedback loop between eutrophication, productivity, and hypoxia. As nitrogen loading and climate-induced stratification intensify, nitrification will likely play an increasingly central role in modulating oxygen dynamics in estuarine systems. Future studies should incorporate seasonal observations, molecular analyses, and sediment flux measurements to refine estimates of microbial oxygen demand and enhance predictive capacity for hypoxia occurrence under changing environmental conditions. Understanding the complex interactions among microbial nitrogen cycling, oxygen dynamics, and anthropogenic inputs is critical for effective estuarine management and for mitigating the ecological impacts of hypoxia in the coastal ocean.

Acknowledgements

We are grateful to Wenbin Zou, Bin Chen and Zuoli

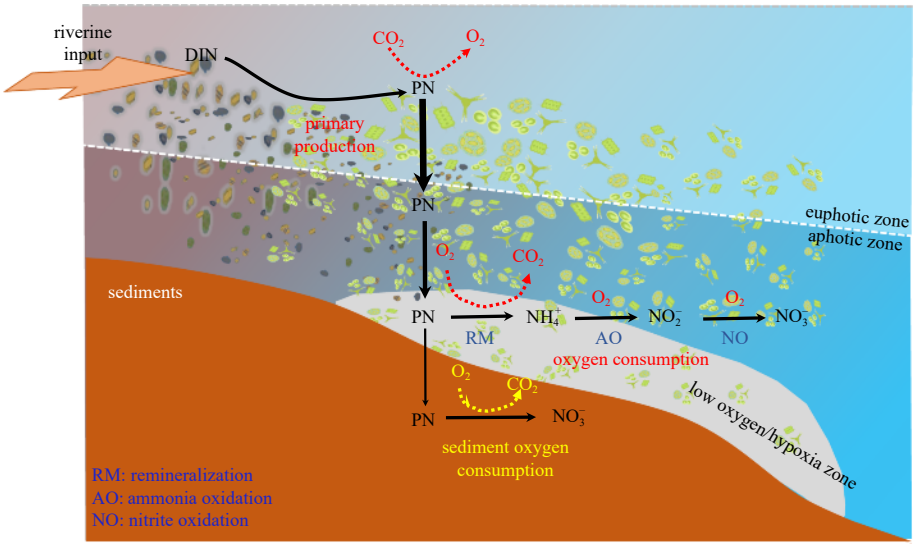

Fig. 9. The conceptual diagram illustrates the interconnected processes of primary production, nitrogen oxidation, and oxygen consumption in the Changjiang River Estuary.

Tan for their assistance during on-board sampling and incubation.

References

Beman J M, Chow C E, King A L, et al. 2011. Global declines in oceanic nitrification rates as a consequence of ocean acidification. Proceedings of the National Academy of Sciences of the United States of America, 108(1): 208–213, doi: 10.1073/pnas.1011053108

Beman J M, Vargas S M, Wilson J M, et al. 2021. Substantial oxygen consumption by aerobic nitrite oxidation in oceanic oxygen minimum zones. Nature Communications, 12(1): 7043, doi: 10.1038/s41467-021-27381-7

Breitburg D, Levin L A, Oschlies A, et al. 2018. Declining oxygen in the global ocean and coastal waters. Science, 359(6371): eaam7240, doi: 10.1126/science.aam7240

Bristow L A, Dalsgaard T, Tiano L, et al. 2016. Ammonium and nitrite oxidation at nanomolar oxygen concentrations in oxygen minimum zone waters. Proceedings of the National Academy of Sciences of the United States of America, 113(38): 10601–10606, doi: 10.1073/pnas.1600359113

Bristow L A, Sarode N, Cartee J, et al. 2015. Biogeochemical and metagenomic analysis of nitrite accumulation in the Gulf of Mexico hypoxic zone. Limnology and Oceanography, 60(5): 1733–1750, doi: 10.1002/lno.10130

Chi Lianbao, Song Xiuxian, Yuan Yongquan, et al. 2020. Main factors dominating the development, formation and dissipation of hypoxia off the Changjiang Estuary (CE) and its adjacent waters, China. Environmental Pollution, 265: 115066, doi: 10.1016/j.envpol.2020.115066

Dai M, Wang L, Guo X, et al. 2008. Nitrification and inorganic nitrogen distribution in a large perturbed river/estuarine system: the Pearl River Estuary, China. Biogeosciences, 5: 1227–1244, doi: 10.5194/bg-5-1227-2008

Dai Xiaofeng, Chen Mingming, Wan Xianhui, et al. 2022. Potential contributions of nitrifiers and denitrifiers to nitrous oxide sources and sinks in China's estuarine and coastal areas. Biogeosciences, 19: 3757–3773, doi: 10.5194/bg-19-3757-2022

Damashek J, Casciotti K L, Francis C A. 2016. Variable nitrification rates across environmental gradients in turbid, nutrient-rich estuary waters of San Francisco Bay. Estuaries and Coasts, 39(4): 1050–1071, doi: 10.1007/s12237-016-0071-7

Diaz R J, Rosenberg R. 2008. Spreading dead zones and consequences for marine ecosystems. Science, 321(5891): 926–929, doi: 10.1126/science.1156401

Ehrich S, Behrens D, Lebedeva E, et al. 1995. A new obligately chemolithoautotrophic, nitrite-oxidizing bacterium, Nitrospira moscoviensis sp. nov. and its phylogenetic relationship. Arch Microbiol, 164: 16–23, doi: 10.1007/BF02568729

Füssel J, Lam P, Lavik G, et al. 2012. Nitrite oxidation in the Namibian oxygen minimum zone. International Society for Microbial Ecology, 6(6): 1200–1209, doi: 10.1038/ismej.2011.178

Galloway J N, Bleeker A, Erisman J W. 2021. The human creation and use of reactive nitrogen: a global and regional perspective. Annual Review of Environment and Resources, 46: 255–288, doi: 10.1146/annurev-environ-012420-045120

Gao Juan, Hou Lijun, Zheng Yanling, et al. 2018. Shifts in the community dynamics and activity of ammonia-oxidizing prokaryotes along the Yangtze estuarine salinity gradient. Journal of Geophysical Research: Biogeosciences, 123(11): 3458–3469, doi: 10.1029/2017JG004182

Granger J, Sigman D M. 2009. Removal of nitrite with sulfamic acid for nitrate N and O isotope analysis with the denitrifier method. Rapid Communications in Mass Spectrometry, 23(23): 3753–3762, doi: 10.1002/rcm.4307

Guisasola A, Jubany I, Baeza J A, et al. 2005. Respirometric estimation of the oxygen affinity constants for biological ammonium and nitrite oxidation. Journal of Chemical Technology & Biotechnology, 80(4): 388–396, doi: 10.1002/jctb.1202

Guo Jie, Jin Yong, Liu Shanwei, et al. 2024. Investigation of the causes and mechanisms of hypoxia in the central Bohai Sea in the summer of 2022. Marine Pollution Bulletin, 206: 116710, doi: 10.1016/j.marpolbul.2024.116710

Heiss E M, Fulweiler R W. 2016. Coastal water column ammonium and nitrite oxidation are decoupled in summer. Estuarine, Coastal and Shelf Science, 178: 110–119, doi: 10.1016/j.ecss.2016.06.002

Hou Xing, Liu Chongcong, Song Guodong, et al. 2025. Nitrogen uptake and nitrification in the Changjiang Estuary. Marine Environmental Research, 209: 107206, doi: 10.1016/j.marenvres.2025.107206

Howarth R W. 2008. Coastal nitrogen pollution: a review of sources and trends globally and regionally. Harmful Algae, 8(1): 14–20, doi: 10.1016/j.hal.2008.08.015

Hsiao S S Y, Hsu T C, Liu J w, et al. 2014. Nitrification and its oxygen consumption along the turbid Chang Jiang River plume. Biogeosciences, 11: 2083–2098, doi: 10.5194/bg-11-2083-2014

Kits K D, Sedlacek C J, Lebedeva E V, et al. 2017. Kinetic analysis of a complete nitrifier reveals an oligotrophic lifestyle. Nature, 549(7671): 269–272, doi: 10.1038/nature23679

Kuypers M M M, Marchant H K, Kartal B. 2018. The microbial nitrogen-cycling network. Nature Reviews Microbiology, 16: 263–276, doi: 10.1038/nrmicro.2018.9

Liu Li, Chen Mingming, Wan X S, et al. 2023. Reduced nitrite accumulation at the primary nitrite maximum in the cyclonic eddies in the western North Pacific subtropical gyre. Science Advances, 9(33): eade2078, doi: 10.1126/sciadv.ade2078

Liu Anqi, Zhou Feng, Ma Xiao, et al. 2024. Inter-annual variations of dissolved oxygen and hypoxia off the northern Changjiang River (Yangtze River) Estuary in summer from 1997 to 2014. Acta Oceanologica Sinica, 43(6): 119–130, doi: 10.1007/s13131-023-2244-0

Lu Yanhong, Cheung Shunyan, Chen Ling, et al. 2020. New insight to niche partitioning and ecological function of am-

monia oxidizing archaea in subtropical estuarine ecosystem. Biogeosciences, 17(23): 6017–6032, doi: 10.5194/bg-17-6017-2020

Ma Xiao, Meng Qicheng, Li Dewang, et al. 2024. Coastal hypoxia response to the coupling of catastrophic flood, extreme marine heatwave and typhoon: a case study off the Changjiang River Estuary in summer 2020. Acta Oceanologica Sinica, 43(6): 107–118, doi: 10.1007/s13131-024-2311-1

Martens-Habbena W, Berube P M, Urakawa H, et al. 2009. Ammonia oxidation kinetics determine niche separation of nitrifying Archaea and Bacteria. Nature, 461: 976–979, doi: 10.1038/nature08465

Nowka B, Off S, Daims H, et al. 2015. Improved isolation strategies allowed the phenotypic differentiation of two *Nitrospira* strains from widespread phylogenetic lineages. FEMS Microbiology Ecology, 91(3): fiu031, doi: 10.1093/femsec/fiu031

Pachiadaki M G, Sintes E, Bergauer K, et al. 2017. Major role of nitrite-oxidizing bacteria in dark ocean carbon fixation. Science, 358(6366): 1046–1051, doi: 10.1126/science.aan8260

Park B J, Park S J, Yoon D N, et al. 2010. Cultivation of autotrophic ammonia-oxidizing archaea from marine sediments in coculture with sulfur-oxidizing bacteria. Applied and Environmental Microbiology, 76(22): 7575–7587, doi: 10.1128/AEM.01478-10

Peng Xuefeng, Fuchsman C A, Jayakumar A, et al. 2016. Revisiting nitrification in the eastern tropical South Pacific: a focus on controls. Journal of Geophysical Research: Oceans, 121(3): 1667–1684, doi: 10.1002/2015JC011455

Qin Wei, Amin S A, Martens-Habbena W, et al. 2014. Marine ammonia-oxidizing archaeal isolates display obligate mixotrophy and wide ecotypic variation. Proceedings of the National Academy of Sciences of the United States of America, 111(34): 12504–12509, doi: 10.1073/pnas.132411511

Schaefer S C, Hollibaugh J T. 2017. Temperature decouples ammonium and nitrite oxidation in coastal waters. Environmental Science & Technology, 51(6): 3157–3164, doi: 10.1021/acs.est.6b03483

Sheng Hui, Darby S E, Zhao Ning, et al. 2024. Anthropogenic eutrophication and stratification strength control hypoxia in the Yangtze Estuary. Communications Earth & Environment, 5(1): 235, doi: 10.1038/s43247-024-01403-w

Sigman D M, Casciotti K L, Andreani M, et al. 2001. A bacterial method for the nitrogen isotopic analysis of nitrate in seawater and freshwater. Analytical Chemistry, 73(17): 4145–4153, doi: 10.1021/ac010088e

Sun Xin, Frey C, Ward B B. 2023. Nitrite oxidation across the full oxygen spectrum in the ocean. Global Biogeochemical Cycles, 37(4): e2022GB007548, doi: 10.1029/2022GB007548

Tang Weiyi, Ward B B, Beman M, et al. 2023. Database of nitrification and nitrifiers in the global ocean. Earth System Science Data, 15(11): 5039–5077, doi: 10.5194/essd-15-5039-2023

Taylor A E, Mellbye B L. 2022. Differential responses of the catalytic efficiency of ammonia and nitrite oxidation to changes in temperature. Frontiers in Microbiology, 13: 817986, doi: 10.3389/fmicb.2022.817986

Wan X S, Sheng Hua-Xia, Liu Li, et al. 2023. Particle-associated denitrification is the primary source of N2O in oxic coastal waters. Nature Commnunications, 14: 8280, doi: 10.1038/s41467-023-43997-3

Wang Hongjie, Dai Minhan, Liu Jinwen, et al. 2016. Eutrophication-driven hypoxia in the East China Sea off the Changjiang Estuary. Environmental Science & Technology, 50(5): 2255–2263, doi: 10.1021/acs.est.5b06211

Wang Wentao, Yu Zhiming, Wu Zaixing, et al. 2018. Rates of nitrification and nitrate assimilation in the Changjiang River Estuary and adjacent waters based on the nitrogen isotope dilution method. Continental Shelf Research, 163: 35–43, doi: 10.1016/j.csr.2018.04.014

Ward B B. 2005. Temporal variability in nitrification rates and related biogeochemical factors in Monterey Bay, California, USA. Marine Ecology Progress Series, 292: 97–109, doi: 10.3354/meps292097

Wei Hengchen, Lin Xianbiao. 2021. Shifts in the relative abundance and potential rates of sediment ammonia-oxidizing archaea and bacteria along environmental gradients of an urban river–estuary–adjacent sea continuum. Science of the Total Environment, 771: 144824, doi: 10.1016/j.scitotenv.2020.144824

Xia Xinghui, Yang Zhifeng, Zhang Xueqing. 2009. Effect of suspended-sediment concentration on nitrification in river water: importance of suspended sediment−water interface. Environmental Science & Technology, 43(10): 3681–3687

Yan Xiuli, Xu Min Nina, Wan X S, et al. 2017. Dual isotope measurements reveal zoning of nitrate processing in the summer Changjiang (Yangtze) River plume. Geophysical Research Letters, 44(24): 12289–12297, doi: 10.1002/2017GL075951

Zhang Wenxia, Wu Hui, Hetland R D, et al. 2019. On mechanisms controlling the seasonal hypoxia hot spots off the Changjiang River Estuary. Journal of Geophysical Research: Oceans, 124(12): 8683–8700, doi: 10.1029/2019JC015322

Zheng Zhenzhen, Wan Xianhui, Xu Min Nina, et al. 2017. Effects of temperature and particles on nitrification in a eutrophic coastal bay in Southern China. Journal of Geophysical Research: Biogeosciences, 122(9): 2325–2337, doi: 10.1002/2017JG003871

Zheng Zhenzhen, Zheng Liwei, Xu Min Nina, et al. 2020. Substrate regulation leads to differential responses of microbial ammonia-oxidizing communities to ocean warming. Nature Communications, 11(1): 3511, doi: 10.1038/s41467-020-17366-3

Zhou Jie, Zheng Yanling, Hou Lijun, et al. 2023. Effects of acidification on nitrification and associated nitrous oxide emission in estuarine and coastal waters. Nature Communications, 14(1): 1380, doi: 10.1038/s41467-023-37104-9